J. Fluid Mech. (1991), *vol.* 226, *pp.* 371–382
Printed in Great Britain

Onset of convection in an anisotropic porous medium with oblique principal axes

By PEDER A. TYVAND[1] AND LEIV STORESLETTEN[2]

[1] Department of Agricultural Engineering, Agricultural University of Norway, 1432 Ås-NLH, Norway

[2] Department of Mathematics, Agder College, 4600 Kristiansand, Norway

(Received 31 May 1990)

We investigate the onset of Rayleigh–Bénard convection in a horizontal porous layer with anisotropic permeability. The permeability is transversely isotropic, whereas the orientation of the longitudinal principal axes is arbitrary. This is sufficient to achieve qualitatively new flow patterns with a tilted plane of motion or tilted lateral cell walls. The critical Rayleigh number and wavenumber at marginal stability are calculated. There are two different types of convection cells (rolls): (i) the plane of motion is tilted, whereas the lateral cell walls are vertical; (ii) the plane of motion is vertical, whereas the lateral cell walls are tilted as well as curved. It turns out that type (i) occurs when the transverse permeability is larger than the longitudinal permeability, and for the converse case type (ii) is preferred.

1. Introduction

Rayleigh–Bénard instability in a porous medium was first studied by Horton & Rogers (1945) and later by Lapwood (1948). They identified the important dimensionless group (the Rayleigh number) and determined its critical value at the onset of convection.

Palm, Weber & Kvernvold (1972) performed an analytical study of the steady supercritical roll motion and the associated heat transfer. Their results were extended numerically to higher Rayleigh numbers by Straus (1974), who also investigated the stability of finite-amplitude convection rolls.

In isotropic porous layers of infinite lateral extent, the preferred motion at the onset of convection is in the form of rolls with square cross-sections. In anisotropic layers this is usually not true. By adopting the physical arguments given by Busse (1981, p. 104) we may predict some of the effects of anisotropy at the onset of convection, provided that the principal axes of the medium are directed along the coordinate axes: let us keep the vertical permeability and the vertical conductivity fixed, and vary the corresponding horizontal quantities. Then an increased horizontal permeability will promote the horizontal motion. This increases the preferred cell width and reduces the critical Rayleigh number. An increased horizontal conductivity will speed up the decay of the local buoyancy force. This increases the preferred cell width and increases the critical Rayleigh number. Reducing the horizontal permeability or conductivity will lead to the opposite effects.

Castinel & Combarnous (1974) performed the first study of the onset of convection in a horizontal layer with anisotropic permeability, and their work was extended by Epherre (1975) to porous layers with anisotropic thermal conductivity. The results in these papers fully conform to the physical arguments given above.

Kvernvold & Tyvand (1979) investigated the supercritical roll motion, its stability and the associated heat transfer. They showed that even a three-dimensional anisotropy does not lead to any new mathematical difficulties compared with isotropy. This is true only as long as one of the principal axes is vertical. This requirement has been maintained in all published work in this field, see the review article by McKibbin (1984) as well as McKibbin (1986) and Nilsen & Storesletten (1990). However, in the present work we will study media where none of the principal axes is vertical.

The present paper is concerned with free convection in an horizontal porous layer with anisotropic permeability. The permeability is transversely isotropic, whereas the orientation of the longitudinal principal axis is arbitrary. For simplicity our analysis is restricted to full isotropy in thermal conductivity. This is sufficient to achieve qualitatively new flow patterns with a tilted plane of motion or tilted lateral cell walls. The mechanical anisotropy causes the tilt. A maximal, purely mechanical tilt angle can be determined directly from Darcy's law. We shall see that the thermal isotropy may reduce the tilt significantly. So if the tilt can be classified as thermo-mechanical, it is always smaller than the corresponding mechanical tilt.

2. Mathematical formulation

We consider a fluid-saturated porous layer which is bounded above and below by two infinite and impermeable horizontal planes. The upper and lower boundaries are separated by a distance h and are at constant temperatures T_0 and $T_0+\Delta T$, respectively. Here the characteristic temperature difference ΔT is positive, which means that the layer is heated from below.

The permeability is transversely isotropic, whereas the longitudinal principal axis (with unit vector $\boldsymbol{i}'$) makes an arbitrary angle with the vertical direction. This means that the permeability perpendicular to this tilted principal axis is isotropic. Let $K_\parallel$ and $K_\perp$ denote the longitudinal and transverse components of the permeability tensor $\boldsymbol{K}^*$:

$$\boldsymbol{K}^* = K_\parallel \boldsymbol{i}'\boldsymbol{i}' + K_\perp(\boldsymbol{j}'\boldsymbol{j}' + \boldsymbol{k}'\boldsymbol{k}'). \tag{1}$$

Here $\boldsymbol{j}'$ and $\boldsymbol{k}'$ are unit vectors along the transverse principal axes. A Cartesian frame of reference is chosen, with x- and y-axes at the lower boundary, where the x-axis is aligned along the horizontal projection of $\boldsymbol{i}'$. The z-axis is directed opposite to gravity. The unit vectors in the x-, y- and z-directions are denoted by $\boldsymbol{i}, \boldsymbol{j}$ and $\boldsymbol{k}$. The anisotropy parameter $\xi = K_\perp/K_\parallel$ is introduced. We define the dimensionless inverse permeability tensor $\boldsymbol{M}$ by the following relation:

$$\boldsymbol{M}\cdot\boldsymbol{K}^* = K_\perp \boldsymbol{E}, \tag{2}$$

where $\boldsymbol{E}$ is the unit tensor. From this definition we have the expression

$$\begin{aligned}\boldsymbol{M} &= \xi\boldsymbol{i}'\boldsymbol{i}' + \boldsymbol{j}'\boldsymbol{j}' + \boldsymbol{k}'\boldsymbol{k}' \\ &= M_{11}\boldsymbol{i}\boldsymbol{i} + M_{13}(\boldsymbol{i}\boldsymbol{k} + \boldsymbol{k}\boldsymbol{i}) + M_{33}\boldsymbol{k}\boldsymbol{k} + \boldsymbol{j}\boldsymbol{j},\end{aligned} \tag{3}$$

where the tensor components are given by

$$M_{11} = \xi\cos^2\beta + \sin^2\beta, \tag{4}$$

$$M_{13} = \tfrac{1}{2}(\xi-1)\sin 2\beta, \tag{5}$$

$$M_{33} = \cos^2\beta + \xi\sin^2\beta. \tag{6}$$

Here β is the angle between the longitudinal direction and the horizontal plane, i.e. the angle between the vectors $\boldsymbol{i}$ and $\boldsymbol{i}'$.

The linearized version of the dimensionless governing equations, according to the Boussinesq approximation, is given by

$$\boldsymbol{M}\cdot\boldsymbol{v}+\nabla p-R\theta\boldsymbol{k}=0, \tag{7}$$

$$\nabla\cdot\boldsymbol{v}=0, \tag{8}$$

$$\frac{\partial\theta}{\partial t}-w=\nabla^2\theta, \tag{9}$$

see Kvernvold & Tyvand (1979), from whom the appropriate units of dimensionless quantities have been borrowed, with the only exception that $K_\perp$ replaces the vertical permeability. The velocity vector is $\boldsymbol{v}=u\boldsymbol{i}+v\boldsymbol{j}+w\boldsymbol{k}$, p is the pressure, t the time and θ is the deviation from the linear temperature distribution at pure conduction. R is the Rayleigh number defined by

$$R=\frac{K_\perp g\gamma h\Delta T}{\kappa\nu}, \tag{10}$$

where g is the gravitational acceleration, γ is the coefficient of thermal volume expansion, κ the thermal diffusivity of the saturated porous medium and ν the kinematic viscosity of the saturating fluid.

By standard manipulations we eliminate the pressure and the horizontal velocity components from the governing equations (7) and (8). Then we eliminate the vertical velocity from the heat equation (9), and end up with the following equation for the perturbation temperature:

$$\left[M_{33}\frac{\partial^2}{\partial x^2}+\xi\frac{\partial^2}{\partial y^2}+M_{11}\frac{\partial^2}{\partial z^2}-2M_{13}\frac{\partial^2}{\partial x\,\partial z}\right]\left(\frac{\partial\theta}{\partial t}-\nabla^2\theta\right)=R\left(\frac{\partial^2\theta}{\partial x^2}+M_{11}\frac{\partial^2\theta}{\partial y^2}\right). \tag{11}$$

Impermeable and perfectly heat-conducting boundaries require that

$$w=\theta=0 \quad \text{at} \quad z=0 \quad \text{and} \quad z=1. \tag{12}$$

By the heat equation (9) these boundary conditions are expressed by temperature alone:

$$\theta=\frac{\partial^2\theta}{\partial z^2}=0 \quad \text{at} \quad z=0 \quad \text{and} \quad z=1. \tag{13}$$

3. Marginal stability and steady convection rolls

At the onset of convection the preferred flow cells tend to arrange themselves such that the tangential permeability along the streamlines is as large as possible. When $\xi<1$ it is clear that motion in the y-direction should be avoided, as its permeability is minimal. Thus we expect convection cells in the (x,z)-plane, independent of y. When $\xi>1$ we have maximum permeability in the y-direction. This indicates that the preferred motion is independent of x.

These physical arguments suggest that the preferred flow patterns at the onset of convection are independent of x or y depending respectively on whether $\xi>1$ or $\xi<1$. In Appendix A this is confirmed numerically by showing that the Rayleigh number in both cases is a local minimum.

3.1. *Case I*: $\xi>1$

In this case β denotes the angle between the x-axis and the direction with minimal permeability. The solution is assumed independent of x, so there are only even orders of the spatial derivatives. Then the problem is easy to solve analytically, as the

preferred mode consists of a single Fourier component vertically. As the horizontal pressure gradient is assumed zero, the x-component of Darcy's law (7) reduces to the relation:

$$\frac{u}{w} = -\frac{M_{13}}{M_{11}}. \tag{14}$$

This velocity ratio being constant means that the motion occurs in tilted planes which make an angle α with the vertical direction. (A simple mental image of this flow pattern is an array of music discs on a shelf, which are tilted due to insufficient support.) The tilt angle is given by

$$\tan\alpha = -\frac{M_{13}}{M_{11}} = \frac{(1-\xi)\tan\beta}{\xi+\tan^2\beta}. \tag{15}$$

α tends to zero if $\xi \to 1$ or if $\beta \to 0$ or $90°$. In the limit $\xi \to \infty$ we have $\tan\alpha = -\tan\beta$, which means that there is no motion in the longitudinal direction. For ξ fixed, the plane of motion obtains its maximum tilt when

$$\tan\beta = \xi^{\frac{1}{2}} \tag{16}$$

and the corresponding maximum value is

$$|\alpha|_{\max} = \arctan\left(\frac{\xi-1}{2\xi^{\frac{1}{2}}}\right). \tag{17}$$

For example, in the case $\xi = 2$, $|\alpha|_{\max} = 19.47°$ is obtained at $\beta = 54.73°$.

The tilt angle α is purely mechanically determined, as it is derived from a component of Darcy's law without any buoyancy terms. It will hereinafter be termed 'the mechanical tilt angle'. As α is completely decoupled from thermal effects, (15) is obviously not restricted to just thermally driven flows: Tyvand (1986) found the same formula as (15) for the tilt angle of free-surface flow cells in a porous medium, with the same type of anisotropy as assumed in the present paper. The mechanical tilt occurs because mechanical forcing of a flow in the vertical direction will generate a passive flow in the x-direction, due to the oblique anisotropy.

From (11) the governing equation in the absence of x-dependence will be

$$\left(\xi M_{11}^{-1}\frac{\partial^2}{\partial y^2}+\frac{\partial^2}{\partial z^2}\right)\left[\frac{\partial}{\partial t}-\left(\frac{\partial^2}{\partial y^2}+\frac{\partial^2}{\partial z^2}\right)\right]\theta = R\frac{\partial^2\theta}{\partial y^2}. \tag{18}$$

The preferred mode of disturbance which satisfies the boundary conditions is given by

$$\theta = \mathrm{e}^{\mathrm{i}my+\sigma t}\sin\pi z. \tag{19}$$

The boundary-value problem defined by (13) and (18) is easily shown to be self-adjoint. Then σ is real and marginal stability is defined by $\sigma = 0$. Substituting (19) into (18) gives the Rayleigh number at marginal stability as a function of the wavenumber m:

$$R = (\xi M_{11}^{-1}m^2+\pi^2)(1+\pi^2/m^2). \tag{20}$$

Onset of convection in a horizontally unbounded layer occurs at the critical Rayleigh number

$$R_{\mathrm{c}} = \pi^2\left[1+\left(\frac{\xi}{\xi\cos^2\beta+\sin^2\beta}\right)^{\frac{1}{2}}\right]^2, \tag{21}$$

which is defined by minimizing (20) with respect to m. The corresponding (critical) value of m is defined by

$$m_c = \pi(\cos^2\beta + \xi^{-1}\sin^2\beta)^{\frac{1}{4}}. \tag{22}$$

From (21) it follows that $R_c \to 4\pi^2$ as $\xi \to 1$. For ξ fixed, R_c obtains its minimum value $4\pi^2$ when $\beta = 0$ and its maximum value $\pi^2(1+\xi^{\frac{1}{2}})^2$ for $\beta = \frac{1}{2}\pi$.

Finally, we note that the horizontal pressure gradient is zero along the plane $z = \frac{1}{2}$. Thus the horizontal flow component here is not forced horizontally, but is a result of vertical forcing acting through the oblique anisotropy.

3.2. *Case II*: $0 < \xi < 1$

In this case β denotes the angle between the x-axis and the direction with maximal permeability. When $\xi < 1$ it turns out that the preferred mode of solution is independent of y. But in order to demonstrate this numerically (see Appendix A), we also include the y-dependence, and consider a solution of the general form

$$\theta = Z(z)\,e^{i(kx+my)+\sigma t}, \tag{23}$$

where the boundary conditions (13) imply that

$$Z(0) = Z''(0) = Z(1) = Z''(1) = 0. \tag{24}$$

The solution (23) substituted into (11) generates a fourth-order ordinary differential equation with constant coefficients. Its general solution is

$$Z(z) = A_1 e^{r_1 z} + A_2 e^{r_2 z} + A_3 e^{r_3 z} + A_4 e^{r_4 z}, \tag{25}$$

where r_1, r_2, r_3 and r_4 are complex roots of the fourth-degree polynomial

$$(-M_{33}k^2 - \xi m^2 + M_{11}r^2 - 2M_{13}ikr)(\sigma - k^2 - m^2 + r^2) + R(k^2 + M_{11}m^2) = 0. \tag{26}$$

The constants A_1, A_2, A_3 and A_4 satisfy the boundary conditions (24), which leads to a linear homogeneous system of algebraic equations. Non-trivial solutions imply that the determinant of the coefficient matrix is zero:

$$\begin{vmatrix} 1 & 1 & 1 & 1 \\ r_1^2 & r_2^2 & r_3^2 & r_4^2 \\ e^{r_1} & e^{r_2} & e^{r_3} & e^{r_4} \\ r_1^2 e^{r_1} & r_2^2 e^{r_2} & r_3^2 e^{r_3} & r_4^2 e^{r_4} \end{vmatrix} = 0. \tag{27}$$

In Appendix B it is shown that the growth rate $\sigma = 0$ at marginal stability. In order to find the critical Rayleigh number R_c we then put $\sigma = 0$ in (26). Given the parameters ξ, β and the wavenumbers k, m, (26) and (27) represent an eigenvalue problem. The eigenvalues are the Rayleigh numbers:

$$R_0 < R_1 < R_2 < \ldots,$$

where the critical Rayleigh number is defined by

$$R_c = \min R_0(\xi, \beta, k, m), \quad k \geqslant 0, m \geqslant 0. \tag{28}$$

On the basis of the physical arguments given at the beginning of this section, it is expected that R_c is obtained at $m = 0$, which means that the steady solutions at convection onset are independent of y. This hypothesis is confirmed numerically in Appendix A.

The eigenvalue problem (26) and (27) is solved numerically for the case $\sigma = m = 0$. Table 1 shows the computed values of R_c for various values of the anisotropy

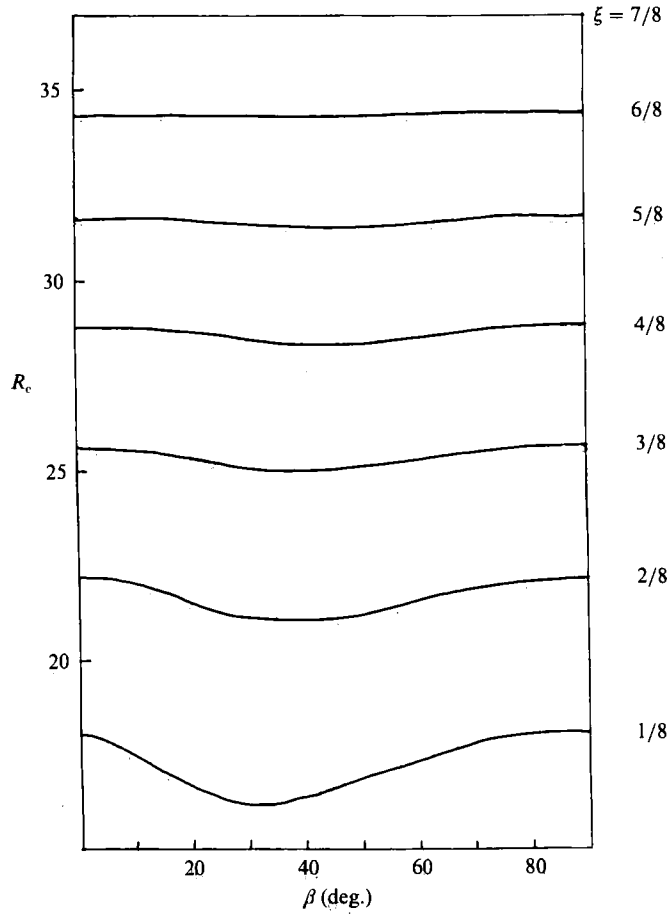

FIGURE 1. The critical Rayleigh number as a function of β for various values of ξ.

ξ... β (deg.)	0.125	0.250	0.375	0.500	0.625	0.750	0.875
0	18.082	22.207	25.658	28.762	31.643	34.367	36.970
10	17.489	21.955	25.535	28.701	31.615	34.356	36.968
20	16.571	21.463	25.268	28.561	31.548	34.330	36.962
30	16.215	21.143	25.053	28.434	31.483	34.303	36.956
40	16.401	21.131	25.000	28.385	31.452	34.289	36.952
50	16.848	21.346	25.100	28.427	31.466	34.292	36.952
60	17.335	21.653	25.282	28.529	31.516	34.312	36.957
70	17.737	21.940	25.472	28.643	31.577	34.337	36.963
80	17.994	22.137	25.609	28.730	31.625	34.358	36.968
90	18.082	22.207	25.658	28.762	31.643	34.367	36.970

TABLE 1. The computed values of R_c for various values of ξ and β

ratio ξ and the angle β. Figure 1 shows the results of table 1 graphically. For given ξ the critical Rayleigh numbers are equal for the cases $\beta = 0$ and $\beta = 90°$, which is known from Kvernvold & Tyvand (1979). Moreover, R_c depends on the angle β, and for each ξ there exists an angle β_m giving a minimum critical Rayleigh number R_m. Table 2

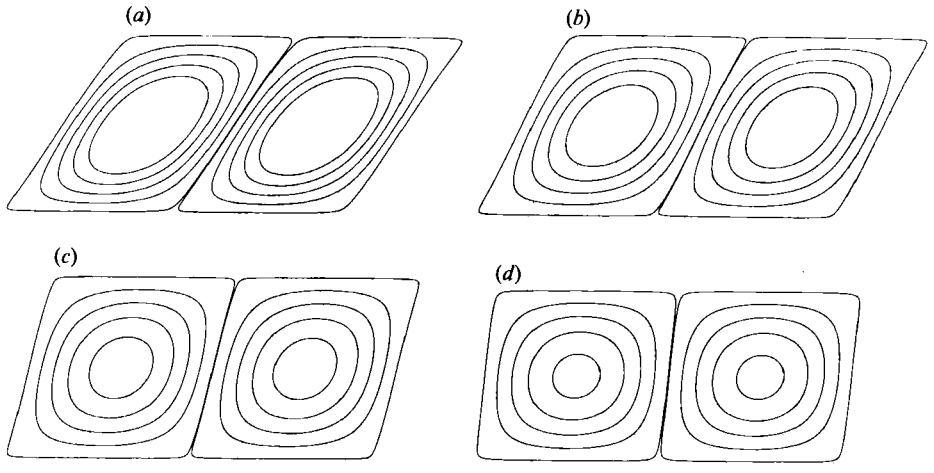

FIGURE 2. Computed streamlines at $\beta = 40.1°$ for the cases (*a*) $\xi = 0.125$, (*b*) 0.25, (*c*) 0.50 and (*d*) 0.75.

ξ	0.125	0.250	0.375	0.500	0.625	0.750	0.875	0.990
β_m (deg.)	30.7	35.2	38.1	39.9	41.4	43.4	44.0	44.9
k_m	2.83	3.00	3.07	3.10	3.12	3.14	3.14	3.14158
R_m	16.214	21.101	24.977	28.385	31.451	34.288	36.952	39.2807

TABLE 2. The computed values of β_m, k_m and R_m for various values of ξ

shows β_m, R_m and the corresponding wavenumber k_m. We observe that $\beta_m \to 45°$ as $\xi \to 1$ ($\xi < 1$). A further look at table 1 confirms that the numbers are almost symmetric about $\beta = 45°$ when ξ is close to one, but develops an asymmetry when ξ is reduced. However, the variation of R_c with β when ξ is fixed is rather small; of order 10% when the variation of the directional permeability covers an order of magnitude.

The computed streamlines are displayed in figure 2 for $\beta = 40.1°$ for the cases $\xi = 0.125$, 0.25, 0.50 and 0.75. A stream function has been defined in order to construct these curves. There is a constant increment in the stream function between two neighbouring streamlines.

A preferred convection cell at the onset of convection will try to arrange itself so that the dominating parts of the flow take place along streamlines with as large a tangential permeability as possible. This may be achieved in two different ways: (i) Selection of the preferred type of motion. When $\xi < 1$ we know that this implies that the motion is independent of y. (ii) Concentration of the flow near the cell boundaries.

In a convection cell with tilt, the flow near the stagnation point in the core follows approximately elliptical streamlines. A relatively large portion of these ellipses have a small tangential permeability. Near the boundaries, however, a much smaller portion of each streamline experiences a small tangential permeability. Most of these outer streamlines have relatively large tangential permeability, and are thus energetically preferable when ξ is small. For β fixed, we may then expect the flow to be more and more concentrated near the cell borders as ξ decreases. This is demonstrated in figure 2. Mathematically this is possible because the preferred eigenfunction is no longer purely sinusoidal (as in case I) but tends to a more rectangular shape.

Stronger anisotropy in case II leads to a stronger concentration of the flow along the borders of the convection cells. This is the quantitatively dominating effect of oblique anisotropy, which is of genuinely thermo-mechanical origin. The tilt itself is of mechanical origin, and can never be enhanced by thermal effects.

We have shown numerically that for ξ and β fixed, the ratio u/w is independent of the x-coordinate at $z = \frac{1}{2}$. This means that all streamlines as well as the lateral cell walls have the same tilt angle at the midplane $z = \frac{1}{2}$. Table 3 shows the ratio u/w and the tilt angle ϕ at $z = \frac{1}{2}$ for various values of ξ, when $\beta = 40.1°$. Here ϕ is defined as the angle between the streamlines at $z = \frac{1}{2}$ and the vertical direction. The fourth line in this table shows the mechanical tilt angle α for comparison.

It is obvious that the x-derivative of the pressure is zero at the stagnation points at the boundaries $z = 0$ and $z = 1$. This fact alone does not say anything about the tilt, as $u = w = 0$ there. However, it is plausible that this horizontal component of the pressure gradient tends to zero more rapidly than the velocity components as we approach the stagnation points along the tilt lines (cell boundaries). We assume that this is true. If so, it implies that the tilt angle is equal to α at the stagnation points at the top and bottom of the layer. This conjecture is hard to prove numerically, but it is not in conflict with the results we have found.

Figure 2 indicates that the tilt lines are curved in S shapes. The reason is that the tilt is reduced by thermal effects. These effects are strongest in the middle of the layer. This is because the flow is primarily pressure driven near the boundaries, while it is primarily buoyancy driven near the middle of the layer.

The tilt lines will achieve maximal curvature when ξ is roughly about 0.2. There are two reasons why the curvature of the tilt lines decreases significantly when ξ is reduced below 0.1: the difference between ϕ and α is reduced, as both of them tend to their common limit value $90° - \beta$; and the tilt lines are stretched as the average tilt increases.

In the present case of purely mechanical anisotropy, the curvature of the tilt lines is hard to visualize clearly. The cases $\xi = 0.125$ and 0.25 in figure 2 are both close to the overall maximum curvature. However, L. Storesletten, in work currently underway, finds a much stronger curvature of tilt lines in his corresponding instability problem where anisotropy in thermal conductivity replaces the present anisotropy in permeability. His work also confirms our present conjecture that the tilt is purely mechanical at the boundaries.

Let us keep β fixed and vary ξ. We start with $\xi = 1$ and reduce it successively down to zero. A plausible hypothesis is that the preferred cell width decreases monotonically with ξ. This may only be true if we define the physical cell width (λ) as the mean distance between two neighbouring cell walls, perpendicularly to the tilt lines. The trouble is that the tilt angle varies, so there are several ways of defining the physical cell width. In table 4 we show the maximum and minimum values of all possible choices of physical cell width. They are defined in the following way:

$$\frac{2\pi}{k_c} = \frac{\lambda_\phi}{\cos\phi} = \frac{\lambda_\alpha}{\cos\alpha}. \tag{29}$$

The left-hand side here is the spatial period of a disturbance, along the x-axis. Table 4 shows that the average physical cell width will usually decrease with decreasing ξ. The physical cell width has a slight tendency to increase with decreasing ξ when we are close to isotropy.

When ξ is not too small, the tilt lines will turn more rapidly with decreasing ξ than the physical cell width will shrink, so that the critical value of k decreases with

ξ	0.125	0.25	0.375	0.50	0.625	0.75	0.875
u/w	0.6563	0.4697	0.3399	0.2416	0.1636	0.0997	0.0459
ϕ (deg.)	33.28	25.16	18.77	13.58	9.29	5.69	2.63
α (deg.)	41.46	33.36	25.89	19.20	13.32	8.21	3.80

TABLE 3. The computed values of u/w and ϕ at $z = \frac{1}{2}$ for various values of ξ, when $\beta = 40.1°$. The angle α (given by (15)) is included for comparison

ξ	0.125	0.25	0.375	0.50	0.625	0.75	0.875	0.99
k_c	3.3560	3.1791	3.1229	3.1061	3.1048	3.1129	3.1259	3.1403
λ_ϕ	1.5652	1.7889	1.9050	1.9663	1.9972	2.0084	2.0079	2.0008
λ_α	1.4031	1.6508	1.8100	1.9133	1.9693	1.9977	2.0056	2.0008

TABLE 4. Physical cell width represented by λ_ϕ and λ_α, as defined in (29). ξ is varied and $\beta = 40.1°$. The critical wavenumber k_c is also included

decreasing ξ. However, this tendency stops when ϕ and α are sufficiently close to $90° - \beta$. From then on, the critical value of k will increase monotonically when ξ is reduced further.

4. Summary and conclusions

The present work is the first study of Rayleigh–Bénard convection in an anisotropic porous medium with oblique principal axes. The analysis is restricted to transversely isotropic media with isotropic thermal conductivity.

Qualitatively new flow patterns occur at the onset of convection. If the transverse permeability is larger than the longitudinal permeability, the planes of motion are tilted, but the cell walls are vertical as usual. On the other hand, if the longitudinal permeability is the larger one, the flow occurs in vertical planes, but the cell walls are tilted. The preference for these different patterns is explained as a preference for flow directions with as small a tangential permeability as possible. This preference also gives rise to a tendency of concentration of the flow along the cell boundaries when the anisotropy increases, in the case when the cell walls are tilted.

The tilt is primarily of mechanical origin, because a vertical forcing due to buoyancy will generate a flow along an oblique principal axis. This flow must have a horizontal component, which causes the tilt. A maximal tilt, which is purely mechanical, occurs when the motion takes place along tilted planes. When the cell walls are tilted, it seems that this maximal tilt will occur at the upper and lower boundaries. In the rest of the layer the tilt is reduced owing to thermal effects, so that the tilted cell walls will be curved. The thermally induced reduction of the tilt is strongest in the middle of the layer.

When the direction of the longitudinal axis is fixed, the critical cell width would be expected to decrease with decreasing ratio between transverse and longitudinal permeability. This will be true only if the cell width is measured perpendicularly to the tilt curves.

The present results have applications in insulation techniques, as described by Kvernvold & Tyvand (1979). The case $0 < \xi < 1$ may be interpreted as a medium composed of parallel fibres. Our results show that there is nothing to be gained by an oblique orientation of the fibres, since the critical Rayleigh number is always reduced

compared with a perpendicular or parallel orientation of fibres *vs.* boundaries. The case $\xi > 1$ may be interpreted as a medium composed of perforated parallel plates: our work confirms the plausible conjecture that the maximal Rayleigh number (i.e. optimal insulating properties) is obtained when these perforated plates are horizontal.

Appendix A

For physical reasons, given in §3, it is expected that the solutions at convection onset are independent of x ($k = 0$) or y ($m = 0$) depending on whether $\xi > 1$ or $\xi < 1$. This is confirmed numerically by showing that the critical Rayleigh number is a local minimum with respect to small variations in m when $\xi < 1$, and with respect to small variations in k when $\xi > 1$. The results are given in the tables below, for the cases $\xi = 0.25$, 0.50, 2.00 and 4.00, with the angle $\beta = 30°$. The number of digits is chosen so that we are able to see all significant variations in R. From these tables we note that the Rayleigh number at marginal stability is not always a local minimum, if the wavenumber is sufficiently far from its preferred value. So our conclusion that the flow at the onset of convection is either independent of x or independent of y, is only valid in a layer of infinite horizontal extent. Convection in a finite box must generally be assumed to be fully three-dimensional.

The case $\xi = 0.25$ and $\beta = 30°$:

	$m = 0$	$m = 0.01$	$m = 0.10$
$k = 2.00$	$R = 23.7479$	$R = 23.7479$	$R = 23.7478$
2.25	22.2313	22.2314	22.2345
2.50	21.4397	21.4397	21.4445
2.75	21.1529	21.1530	21.1586
3.00	21.2390	21.2390	21.2452
3.25	21.6146	21.6146	21.6211
3.50	22.2252	22.2252	22.2318
3.75	23.0338	23.0338	23.0405
4.00	24.0146	24.0147	24.0213

The case $\xi = 0.50$ and $\beta = 30°$:

	$m = 0$	$m = 0.01$	$m = 0.10$
$k = 2.00$	$R = 32.7444$	$R = 32.7443$	$R = 32.7343$
2.25	30.4335	30.4335	30.4311
2.50	29.1370	29.1370	29.1389
2.75	28.5399	28.5400	28.5443
3.00	28.4529	28.4530	28.4588
3.25	28.7564	28.7565	28.7632
3.50	29.3721	29.3722	29.3795
3.75	30.2469	30.2470	30.2546
4.00	31.3436	31.3437	31.3516

The case $\xi = 2.00$ and $\beta = 30°$:

	$k = 0$	$k = 0.01$	$k = 0.10$
$m = 2.00$	$R = 50.0729$	$R = 50.0727$	$R = 50.0606$
2.25	46.1762	46.1762	46.1747
2.50	43.8775	43.8775	43.8818
2.75	42.6726	42.6726	42.6802
3.00	42.2581	42.2582	42.2677
3.25	42.4427	42.4429	42.4535
3.50	43.1009	43.1010	43.1124
3.75	44.1475	44.1476	44.1594
4.00	45.5229	45.5231	45.5352

The case $\xi = 4.00$ and $\beta = 30°$:

	$k = 0$	$k = 0.01$	$k = 0.10$
$m = 2.00$	$R = 51.2922$	$R = 51.2923$	$R = 51.3042$
2.25	47.4889	47.4890	47.5042
2.50	45.2946	45.2947	45.3113
2.75	44.2050	44.2052	44.2222
3.00	43.9170	43.9171	43.9342
3.25	44.2390	44.2391	44.2560
3.50	45.0455	45.0457	45.0623
3.75	46.2514	46.2515	46.2679
4.00	47.7972	47.7974	47.8135

Appendix B. A proof of the principle of exchange of stabilities ($\sigma_i = 0$)

The solution of (18) at convection onset may be written

$$\begin{aligned}\theta &= \mathrm{Re}\{Z(z)\,\mathrm{e}^{\mathrm{i}(kx+my+\sigma_i t)}\}\\ &= \mathrm{Re}\{Z^*(z)\,\mathrm{e}^{-\mathrm{i}(kx+my+\sigma_i t)}\},\end{aligned} \tag{B 1}$$

where the asterisk denotes complex conjugate and σ_i the imaginary part of the growth rate. The boundary conditions (19) may be written

$$\frac{\mathrm{d}^2 Z}{\mathrm{d}z^2} = \frac{\mathrm{d}^2 Z^*}{\mathrm{d}z^2} = Z = Z^* = 0 \quad \text{at} \quad z = 0, 1. \tag{B 2}$$

The following notation is introduced:

$$\langle\ \rangle = \int_0^1 (\ )\,\mathrm{d}z. \tag{B 3}$$

We have two alternative forms (B 1) of the solutions of (18). Both of the solutions are taken in full complex form and substituted into this equation. The two resulting equations are multiplied by Z and Z^*, respectively, and integrated over the layer. These equations are subtracted from each other. Partial integration and application of the boundary condition (B 2) finally produces the equation

$$\begin{aligned}2k\sigma_i M_{13}\left\langle Z^*\frac{\mathrm{d}Z}{\mathrm{d}z}\right\rangle - \mathrm{i}\sigma_i(M_{33}k^2+\xi m^2)\langle|Z|^2\rangle + \mathrm{i}\sigma_i M_{11}\left\langle\left|\frac{\mathrm{d}Z}{\mathrm{d}z}\right|^2\right\rangle\\ = \mathrm{i}kM_{13}\left(\left|\frac{\mathrm{d}Z}{\mathrm{d}z}\right|^2_{z=1} - \left|\frac{\mathrm{d}Z}{\mathrm{d}z}\right|^2_{z=0}\right).\end{aligned} \tag{B 4}$$

From this equation it is obvious that $\sigma_i = 0$.

REFERENCES

BUSSE, F. H. 1981 Transition to turbulence in Rayleigh–Bénard convection. In *Hydrodynamic Instabilities and the Transition to Turbulence* (ed. H. L. Swinney & J. P. Gollub), pp. 97–137. Springer.

CASTINEL, G. & COMBARNOUS, M. 1974 Critere d'apparition de la convection naturelle dans une couche poreuse anisotrope. *C. R. hebd. Séanc. Acad. Sci. Paris* B **287**, 701–704.

EPHERRE, J. F. 1975 Critere d'apparition de la convection naturelle dans une couche poreuse anisotrope. *Rev. Gén. Thermique* **168**, 949–950.

HORTON, C. W. & ROGERS, F. T. 1945 Convection currents in a porous medium. *J. Appl. Phys.* **16**, 367–370.

KVERNVOLD, O. & TYVAND, P. A. 1979 Nonlinear thermal convection in anisotropic porous media. *J. Fluid Mech.* **90**, 609–624.

LAPWOOD, E. R. 1948 Convection of a fluid in a porous medium. *Proc. Camb. Phil. Soc.* **44**, 508–521.

MCKIBBIN, R. 1984 Thermal convection in layered and anisotropic porous media: a review. In *Convective Flows in Porous Media* (ed. R. A. Wooding & I. White), pp. 113–127. DSIR, Wellington, New Zealand.

MCKIBBIN, R. 1986 Thermal convection in a porous layer: Effects of anisotropy and surface boundary conditions. *Transport Por. Media* **1**, 271–292.

NILSEN, T. & STORESLETTEN, L. 1990 An analytical study on natural convection in isotropic and anisotropic porous channels. *Trans. ASME* C: *J. Heat Transfer* **112**, 396–401.

PALM, E., WEBER, J. E. & KVERNVOLD, O. 1972 On steady convection in a porous medium. *J. Fluid Mech.* **64**, 153–161.

STRAUS, J. M. 1974 Large amplitude convection in porous media. *J. Fluid Mech.* **64**, 51–63.

TYVAND, P. A. 1986 Decay of a disturbed free surface in an anisotropic porous medium. *J. Hydrol.* **83**, 367–371.